Modified Graphene Oxide-Zinc Oxide Assisted Accelerated Photodegradation of Polystyrene under Ultraviolet Irradiation

S. Dinoop Lal[1,], T. Sunil Jose[1,*,], C. Rajesh[2], P. Anju Rose Puthukkara[1,], K.J. Rijoy[1,] and K. Savitha Unnikrishnan[1]

[1]Department of Chemistry, St. Thomas College, Thrissur-680001, India
[2]Department of Chemistry, MES Kalladi College, Palakkad-678583, India

*Corresponding author: E-mail: suniljosestc@gmail.com

In this work, the photodegradation of polystyrene (PS) was investigated using modified graphene oxide-zinc oxide (ZnO-GO) photocatalyst under ultraviolet radiation. The optical band gap energy of ZnO decreased in ZnO-GO composites. Photodegradation of PS, PS-ZnO and PS-ZnO-GO composites were studied under artificial UV radiation. PS-ZnO-GO composites underwent superior chain scission compared to PS-ZnO and pristine PS, upon UV exposure, as evident from gel permeation chromatography (GPC). FTIR spectra revealed the existence of strong chemical interaction between ZnO and GO in the prepared composites. Moreover, FTIR spectroscopy substantiated the occurrence of photo-oxidation in PS chains upon UV exposure. The decrease in the mechanical properties, dielectric breakdown voltage and thermal stability the irradiated specimens demonstrating the spread of degradation of PS chain to the inner matrix from the surface. Considering the results of all the analysis techniques, it was evident that PS-ZnO-GO composites underwent superior photodegradation compared to PS-ZnO and pristine PS. A possible mechanism of degradation was also proposed.

Keywords: Zinc oxide, Graphene oxide, Hydrothermal method, Photodegradation, Dielectric breakdown, Mechanical properties.

INTRODUCTION

The 20th century seen extensive commercialization of polymers, which supplanted numerous commodities and machinery. Demand and production of widely used plastics, increased globally reaching up to about 2 metric tons in 1950 [1]. During past 50 years, around 9200 million metric tons of plastics were produced out of which 6900 million metric tons ended up in land fillings [2]. It is estimated that about 79% of the total plastics produced end up as plastic debris in the environment [3]. Most of the plastics being non-biodegradable, remain in the environment as such for several years. Accumulation of plastic debris over the years led to serious environmental issues threatening the ecosystem [4]. Recycling and combustion cannot be implemented as a successful technique for plastic waste elimination. One of the technique that could be developed for plastic waste remediation is photodegradation. Deterioration of materials in the presence of electromagnetic radiation is referred to as photodegradation. Most of the polymers undergo photodegradation in the presence of sunlight without the production of any hazardous side products. The process is cost efficient and ecofriendly.

Polystyrene (PS) undergo phodegradation in the ultraviolet (UV) region of spectra [1,5,6]. Photodegradation of PS require several years to complete, however, the process could be accelerated in the presence of photocatalysts [7]. Inorganic metal oxides like ZnO are widely used as photocatalyst in several environmental remediation applications [8,9]. Metal oxides like ZnO are semiconductors that generated electron-hole pair when exposed to electromagnetic radiation of certain frequencies. Photogenerated electron-hole pairs are responsible for the photocatalytic activity of these materials. Electrons get excited from valance band to conduction band of ZnO when exposed to UV radiation. The photogenerated electrons and holes reacts with oxygen and water molecules respectively, adsorbed on the surface of ZnO particles, creating radicals/ions that are highly reactive. These reactive unstable species interacts with the pollutants like polymers, dyes or other toxic materials initiating degradation [10]. The efficiency of ZnO is however reduced due to factors like charge recombination, photo-corrosion

(conversion of ZnO to Zn(OH)$_2$ under UV light), *etc*. In addition to this, ZnO is soluble in strong acid and alkaline media [11,12]. In order to use ZnO as an effective catalyst in polymer degradation, efficiency of ZnO has to be enhanced. This could be done primarily by minimising the rate of charge recombination in ZnO so that the electrons and holes get enough life time to initiate degradation reaction. Charge carrier lifetime could be maximized by coupling ZnO with other materials that could temporarily accept and stabilize electrons from its conduction band.

Several authors reported the enhancement in photocatalytic efficiency of metal oxide semiconductors when coupled with carbon materials like graphene [13], fullerenes [14] and carbon nanotubes [15]. Graphene is a 2D planar material with large surface area and could be easily prepared compared to carbon nanotubes and fullerenes [16,17]. Graphene also shows better mechanical [18], optical, electronic, magnetic, transport [19], thermal [20], *etc.* properties, in addition to the possibility of tuning their chemical properties by functionalization [21]. In addition to this, superior strength and flexibility of graphene makes it a suitable material for application in various fields like medicine [22], electronics [23], solar cells [24], capactors [25], sensors [26], *etc.* Graphite is oxidized and exfoliated into graphene oxide (GO) layers followed by their reduction to graphene in this technique [27]. GO consists of hydroxyl, epoxy or/and carboxylic acid groups covalently bonded to the carbon atoms of graphene through oxygen [28]. Even though GO resemble graphene in several properties, they are more hydrophilic than the later. The functional groups in GO provides better interaction with polar solvents like water and hence highly dispersible in water compared to graphene [29]. Metal oxide coupled GO has been used as catalysts in environmental remediation applications. The metal-carbon (M-C), metal-oxygen-carbon (M-O-C) and hydrogen bonds were reported to exist between metal oxide and GO in their composites [30-32]. M-C and M-O-C bonds facilitates better charge transport across metal oxide and GO, which changes the electronic and optical properties of the MO-GO composite, making them suitable for superior photocatalytic applications [33]. Decrease in optical band gap energy has been reported in metal oxides when coupled with GO [34]. The catalytic activity of metal oxides could be converted from UV active to visible active by narrowing their optical band gap [35]. This is significant because solar radiation reaching earth surface composes of only 5% UV light and about 45% is visible light.

Through this work, photodegradation of polystyrene (PS) is studied using GO coupled ZnO photocatalyst. The electrical, mechanical, optical and thermal properties of PS, PS-ZnO and PS-ZnO-GO composites were investigated. A thorough investigation of these properties will help in the classification of PS-composites in various applications, industrially. Structure and bonding in ZnO-GO composites are investigated in order to understand the possible mechanism of PS degradation in their presence.

EXPERIMENTAL

Zinc nitrate hexahydrate [Zn(NO$_3$)$_2$·6H$_2$O], graphite (150 mesh), sulphuric acid (98%), sodium nitrate, hydrogen per-

oxide (30% w/v), potassium permanganate and hydrochloric acid were purchased from Merck India Pvt. Ltd. Polystyrene beads were purchased from LG Polymer India Pvt. Ltd. The UV tube (253 nm. 30 W, Phillips Holland) fit inside a wooden chamber was used as UV light source. All the chemicals were used without further purification.

Instrumentation: Powder X-ray diffractometer (XRD), Aeris, Panalytical was used to study the crystal structure through X-ray diffraction of the samples. Copper-Kα radiation (λ = 0.154 nm) was the source of X-ray. IRAffinity-1S, Shimadzu, Japan, was used to identify the molecular structure and study the chemical properties/changes of the specimens through IR spectroscopy. The instrument worked on attenuated total reflection (ATR) mode. UV-visible spectra was obtained from UV-visible diffused reflectance spectrometer (UV-DRS) UV-2600, Shimadzu, Japan. Particle size and morphology was studied using scanning electron microscope (SEM), JSM-6390LV, Jeol and high resolution transmission electron microscope (HRTEM), JEM 2100, Jeol. Elemental analysis was done using energy dispersive X-ray (EDX) machine, Oxford XMX N attached with SEM instrument. Selected area electron diffraction (SAED) patterns were obtained from HRTM instrument. Average molecular weight of the polymer composites were determined using gel permeation chromatography (GPC) instrument, LC-20AD, Shimadzu, Japan. Universal testing machine (UTM), Autograph AG-X plus, Shimadzu, Japan was used to measure tensile and flexural properties of the polymer specimens. Injection moulded polymer specimens was used for mechanical measurements in UTM. Thermal property of polymer composites were studied using Thermogravimetric analysis (TGA) of the specimens was done using the instrument STA 6000, Perkin-Elmer in nitrogen atmosphere. For the determination of dielectric breakdown, a specially designed wooden chamber was setup. The disk like polymer specimens were placed in between two sphere headed copper electrodes connected to the two terminals of an AC source. The chamber was filled with transformer oil and voltage was increased gradually until the specimen broke down.

Synthesis of zinc oxide (ZnO) nanoparticles: Sonication assisted hydrothermal method was adopted for the synthesis of ZnO nanoparticles. Zn(OH)$_2$ was precipitated out from its precursor Zn(NO$_3$)$_2$·6H$_2$O (0.65 g) in 25 mL distilled water by slow addition of ammonia solution at pH 7.5, maintaining a constant stirring. This was sonicated for 1 h using a probe sonicator (750 W). The solution was transferred into a 25 mL Teflon lined hydrothermal autoclave and kept in a hot air oven for 12 h at 130 ºC. The resultant solution was filtered and dried at 80 ºC for 24 h followed by calcination at 400 ºC for 5 h to obtain ZnO nanoparticles [36].

Synthesis of graphene oxide (GO): Graphene oxide (GO) was prepared using modified Hummer's method from graphite (150 mesh) as reported method [37,38].

Preparation of graphene oxide modified zinc oxide (ZnO-GO) composites: Sonication assisted hydrothermal method was used for the preparation of ZnO-GO composites. Three ZnO-GO composites were prepared namely ZnO-3% GO, ZnO-10% GO and ZnO-30% GO, containing 3, 10 and 30 wt.% of GO, respectively with respect to ZnO. In this approach, ZnO

was precipitated in water medium containing dispersed GO. In order to prepare ZnO-3% GO, typically 1 g $Zn(NO_3)_2 \cdot 6H_2O$ was added to the dispersion of GO in water prepared by probe sonicating 40 mL water containing 30 mg GO, for 2 h. $Zn(OH)_2$ was precipitated by slow addition of ammonia while stirring the solution vigorously. This was transferred into a 25 mL Teflon lined hydrothermal autoclave and kept in a hot air oven for 6 h at 130 ºC. The product obtained was filtered, washed with distilled water several times and dried in a hot air oven at 70 ºC for 12 h. Same method was followed for the preparation of ZnO-10% GO and ZnO-30%, altering the weight of $Zn(NO_3)_2 \cdot 6H_2O$ used while keeping the weight of GO constant. For the preparation of ZnO-10% GO and ZnO-30% GO, weights of $Zn(NO_3)_2 \cdot 6H_2O$ taken were 300 mg and 100 mg, respectively [39].

Preparation of polystyrene and polystyrene-photocatalyst composite sheets: Polystyrene (PS) sheets were developed from PS beads by solvent casting as described earlier [40]. PS beads were dissolved in toluene solvent, homogenized using ultrasonic probe sonicator (750 W), casted into petridish and dried into PS sheets. PS-3% ZnO, PS-3% (ZnO-3% GO), PS-3% (ZnO-10% GO) and PS-3% (ZnO-30% GO) composite films were prepared by loading 3 wt.% of respective photocatalysts into PS dissolved in toluene and following the above procedure. The PS-photocatalyst sheets hence prepared were subjected to photodegradation studies.

Preparation of polystyrene and polystyrene composite sheets for electrical and mechanical studies: In order to prepare specimens for electrical and mechanical studies, PS beads and photocatalyst fillers were fed into a brabender and mixed thoroughly at 180 ºC. These were cut into the size of small beads and moulded into specimens of various shapes for electrical and mechanical measurements. Inorder to measure electrical properties (dielectric breakdown), the above prepared beads were subjected to hydraulic hot press in a steel mould. Disk shaped specimens of uniform thickness 1 mm and diameter 75 mm were obtained. For mechanical (tensile and flexural) measurements, the beads obtained above was subjected to injection moulding. Bar shaped specimens (ISO-178 standard) were obtained for flexural property measurement and dumbbell like specimens (ISO-527-2-1A) were obtained for measurement of tensile property.

Photodegradation studies: Artificial UV source was used for photodegradation studies. UV tube (30 W, Philips Holland) of wavelength 253 nm was fixed in a wooden chamber, which served as UV chamber. The PS/PS-composites were exposed to UV light inside the chamber for 1000 h. At regular intervals of 200 h, the specimens were taken out for various analysis to monitor photodegradation.

RESULTS AND DISCUSSION

X-ray Studies: X-ray diffractogram of graphite exhibited its characteristic high intense peaks corresponding to (002) and (004) planes at 2θ angles 26.6º and 54.5º, respectively (Fig. 1). Diffractogram of GO on the other hand displayed a sharp and intense peak attributing to (001) plane at 2θ angle 10.8º.
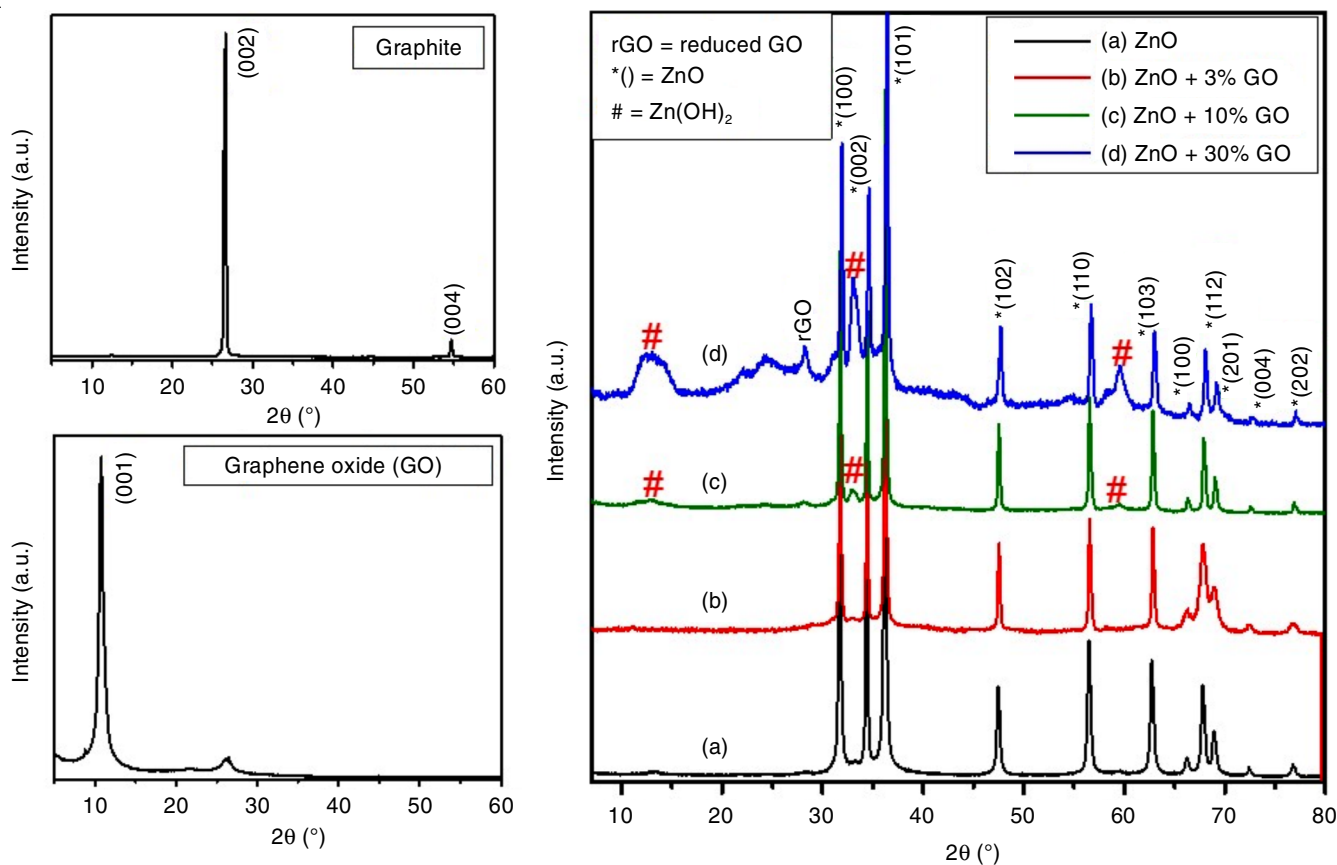

Fig. 1. Powder XRD pattern of graphite, GO and ZnO-GO composites

TABLE-1
CALCULATED INTER PLANAR DISTANCE (d) CORRESPONDING TO THE 2θ ANGLES OBTAINED FROM THE
XRD PATTERN OF ZnO AND ZnO-GO COMPOSITES (CALCULATED USING BRAGG'S EQUATION)

ZnO	2θ (°)	31.9	34.6	36.5	47.7	56.8	63	66.5	68	69.2	72.7	77
	d (Å)	2.8	2.59	2.46	1.9	1.62	1.47	1.41	1.38	1.36	1.3	1.24
ZnO-3% GO	2θ (°)	31.98	34.65	36.47	47.73	56.77	63.05	66.5	68.07	69.2	72.73	77.03
	d (Å)	2.79	2.59	2.46	1.9	1.6	1.47	1.4	1.38	1.36	1.3	1.24
ZnO-10% GO	2θ (°)	31.98	34.65	36.47	47.73	56.77	63.05	66.5	68.07	69.2	72.73	77.03
	d (Å)	2.79	2.59	2.46	1.9	1.6	1.47	1.4	1.38	1.36	1.3	1.24
ZnO-30% GO	2θ (°)	31.98	34.65	36.47	47.73	56.77	63.05	66.5	68.07	69.2	72.73	77.03
	d (Å)	2.79	2.59	2.46	1.9	1.6	1.47	1.4	1.38	1.36	1.3	1.24

The characteristic diffraction peaks of graphite were absent in the prepared GO. This showed that all the graphite used in the reaction had be entirely converted into GO. In addition to the characteristic peak corresponding to (001) plane of GO, another low intense broad pattern centred at 2θ angle 26.1° was also observed. This represents the presence of reduced graphene oxide (rGO) in traces in the sample. Prepared ZnO showed diffraction peaks at 2θ angles 31.9° (100), 34.6° (022), 36.5° (101), 47.7° (102), 56.8° (110), 63.0° (103), 66.5° (100), 68.0° (112), 69.2° (201), 72.7° (004) and 77.00° (202). These peaks confirm the existence of ZnO in hexagonal wurtzite crystal structure [40]. From Fig. 1, it was evident that the diffractogram of ZnO-GO composites, exhibited all the peaks corresponding to ZnO. The well distinguishable sharp patterns of ZnO reveals that the crystalline morphology of ZnO remained intact upon coupling with GO. The composites also exhibited crystalline nature. It was also evident that in ZnO-GO composites, as the percentage of GO increased (from 3% to 30%), amorphous character increased slightly. The presence of rGO was clear in ZnO-GO composites with higher percentage of GO. In addition to these peaks, $Zn(OH)_2$ diffraction peaks were also visible at 2θ angles 12.7°, 33.0° and 59.7°. Inter planar distance (d) calculated for ZnO-GO composites were smaller compared to that of pristine ZnO (Table-1). Crystallite sizes of ZnO and ZnO-3% GO, ZnO-10% GO and ZnO-30% GO composites were 30.7 nm, 38.65 nm, 38.83 nm and 38.99 nm respectively as determined using Debye Scherrer's equation [41]. Crystallite size showed an increase in the ZnO-GO composites compared to pristine ZnO (Table-2).

TABLE-2
CRYSTALLITE SIZE OF ZnO AND ZnO-GO
CALCULATED USING DEBYE-SCHERRER EQUATION

	Crystallite size (nm)
ZnO	30.70
ZnO-3% GO	38.65
ZnO-10% GO	38.83
ZnO-30% GO	38.99

Morphological studies: Synthesized ZnO existed as spherical particles having an average diameter of about 80 nm (Fig. 2a) as evident from FESEM image. ZnO-30% GO composite on the other hand showed the existence of ZnO as hexagonal rods with varying sizes, associated with GO. The length of ZnO rods varied from 80 to 650 nm (Fig. 2c). From the EDX pattern of ZnO, the presence of zinc was observed as peaks positioned at 1.02, 8.62 and 9.58 keV and that of oxygen was observed as a peak positioned at 0.53 keV (Fig. 2b). Atomic percentages of zinc and oxygen were found to be 42.04 and 57.96%, respectively. EDX pattern of ZnO-30% GO composite showed the presence of carbon peak positioned at 0.277 keV in addition to the zinc and oxygen peaks (Fig. 2d). Atomic percentages of zinc, oxygen and carbon in the composite were found to be 18.31, 34.18 and 47.51%, respectively. EDX also confirms the purity of prepared ZnO and ZnO-GO composite.

HRTEM image of ZnO-30% GO composites further supported the fact that ZnO existed in the composite as rods associated with GO sheets. These GO sheets held ZnO rods together and also wound around them, capping them (Fig. 3a-b). Lattice fringes corresponding to the (100) plane of ZnO were observed with a lattice spacing of 0.28 nm (Fig. 3c). Halo rings with faded edges were observed in the SAED pattern of the composite due to is amorphous nature. However, the few distinguishable bright spots present over the halo ring reveals its crystalline nature (Fig. 3d). The composite therefore was neither perfect crystalline nor amorphous. The few bright spots observed over the halo rings were identified to be the (102), (110) and (202) plane of ZnO. In addition to this, the spot corresponding to rGO was also identified.

FTIR spectral studies: From the FTIR spectra of ZnO, the vibrations corresponding to stretching and bending modes of H_2O were observed in addition to that of ZnO molecule (Fig. 4). While the stretching band corresponding to Zn-O was observed at the frequency 851 cm^{-1}, the asymmetric and symmetric stretching bands of H-O-H was observed at 3863 and 3741 cm^{-1}, respectively. The stretching band corresponding to O-H was observed as a broad band between 3600-3015 cm^{-1}, while the bending (scissoring) mode of H-O-H was also observed at 1520 cm^{-1}. It was therefore obvious that water molecules were being adsorbed on the surface of ZnO. The FTIR of GO showed vibrational peaks corresponding to C=O (1720 cm^{-1}), C=C (1620 cm^{-1}), aromatic C=C (1526 cm^{-1}), C-O (1200 and 1055 cm^{-1}), epoxy C-O-C- (961 cm^{-1}), C-H out of plane bend (675 cm^{-1}) and O-H (3600-3000 cm^{-1}). An interesting observation made from the FTIR spectra of ZnO-GO composites in comparison with that of GO was that some of the characteristic vibration bands of GO underwent a considerable shift towards lower wavenumber in the composites. As the percentage of ZnO increased in the composites (moving from ZnO-30% GO to ZnO-3% GO), the stretching vibrations corresponding to C=O and C-O underwent a shift in peak positions towards lower
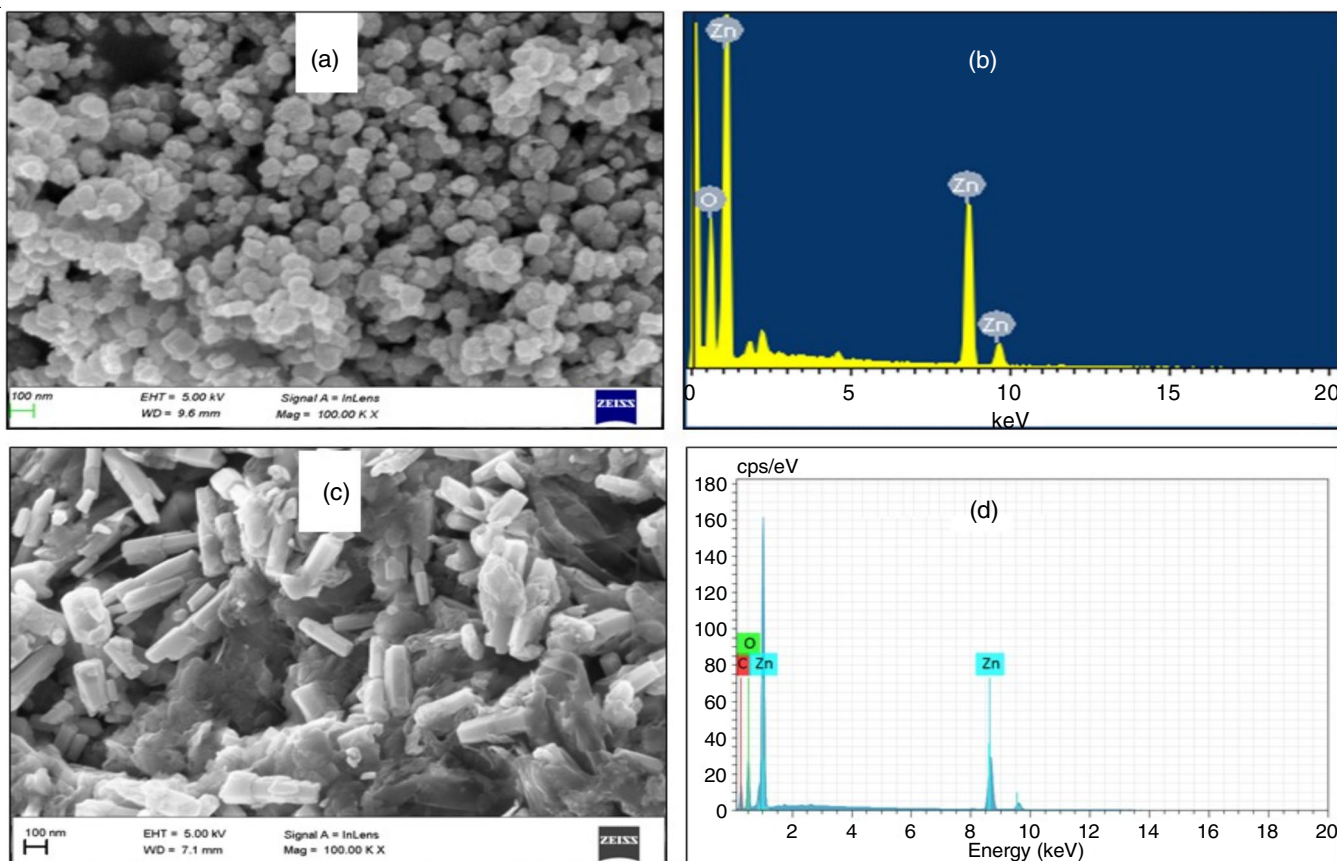
Fig. 2. FESEM image of (a) ZnO and (c) ZnO-30% GO composite. EDX pattern of (b) ZnO and (d) ZnO-30% GO composite
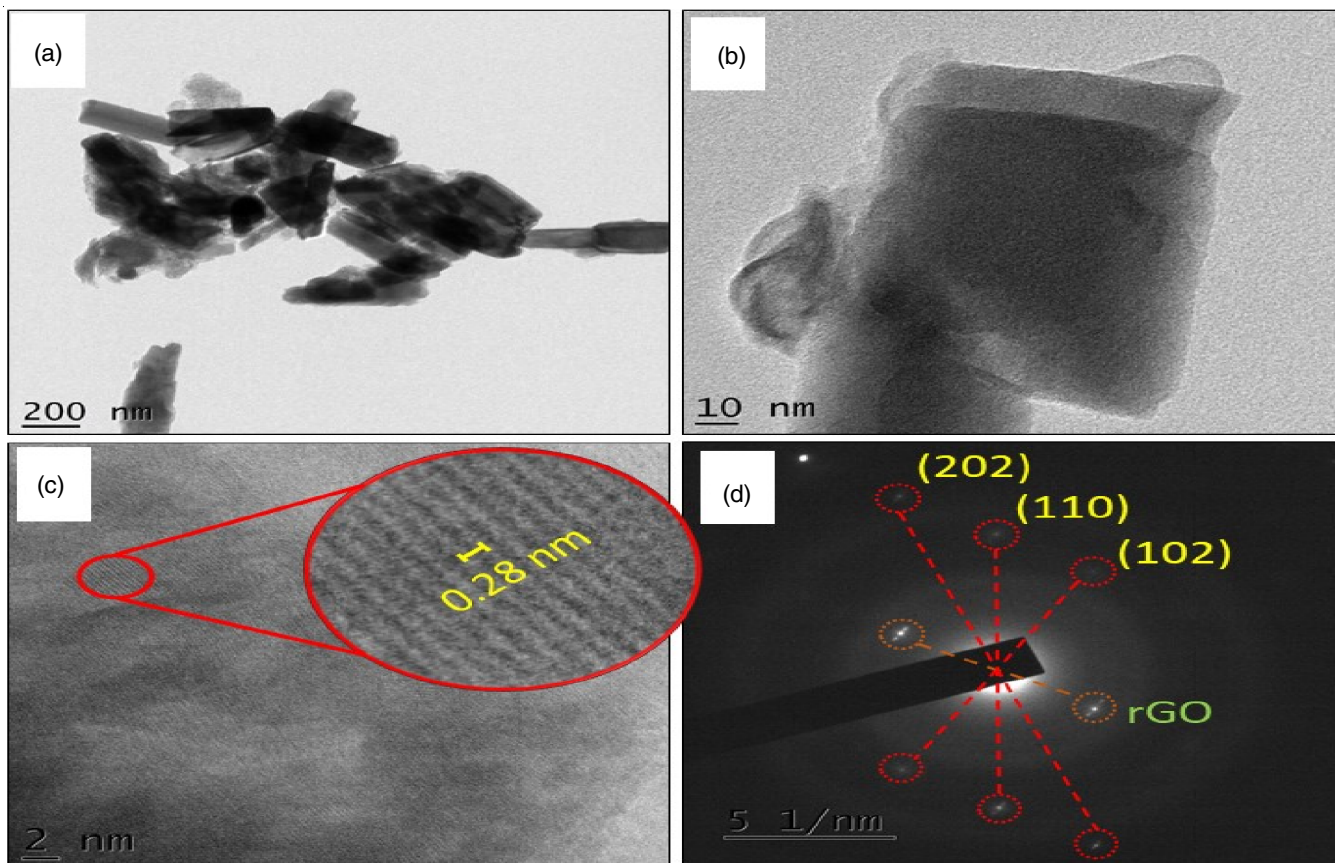

Fig. 3. HRTEM image (a, b and c) and SAED pattern (d) of ZnO-30% GO composite
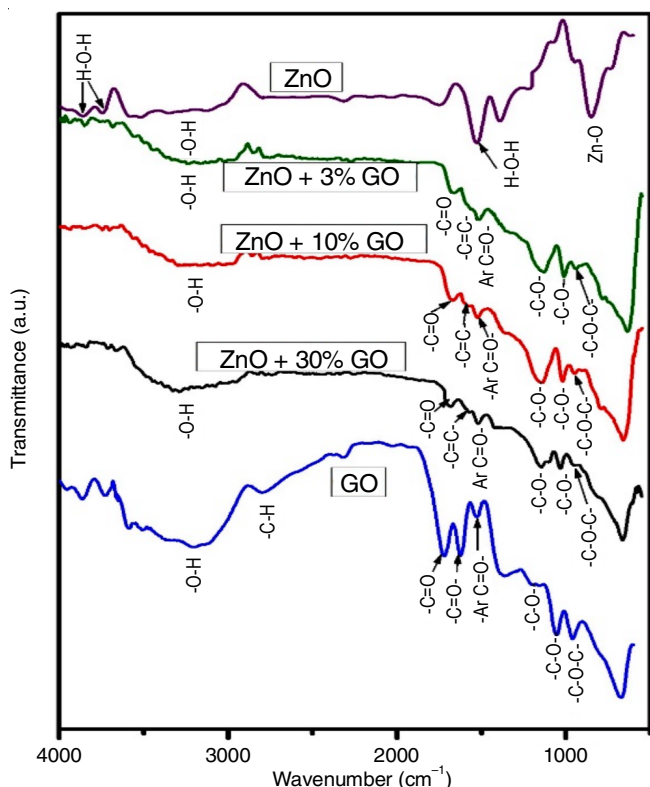
Fig. 4. FTIR spectra of ZnO, GO and ZnO-GO composites

wavenumber. This observation suggests the existence of a strong chemical bonding interaction between ZnO and the oxygen atom of C=O/C-O groups of GO. Table-3 shows the tabulated data of major peaks observed in the FTIR spectra of ZnO-GO composites in comparison with GO.

TABLE-3 IMPORTANT PEAKS OBSERVED IN THE FTIR SPECTRA (cm⁻¹) OF GO AND ZnO-GO COMPOSITES				
	GO	ZnO + 30% GO	ZnO + 10% GO	ZnO + 3% GO
>C=O (stretch)	1720	1694	1666	1660
>C=C< (stretch)	1620	1590	1590	1585
Ar-C=C (stretch)	1526	1524	1523	1522
-C-O- (stretch)	1200	1146	1139	1128
-C-O- (stretch)	1055	1030.	1018	1008
-C-O-C- (stretch in epoxide)	961	951	947	943

Optical studies: ZnO absorbed in the UV region (λ < 400 nm) with no absorption in the visible region (400-800 nm) where as ZnO-GO composites showed absorption in UV as well as visible region (Fig. 5a). The optical band gap energy (E_g) ZnO and ZnO-GO composites were determined using Tauc plote. Kubelka-Munk function (F(R)) was initially determined from reflectance spectra of the composites using the following relation [42]:
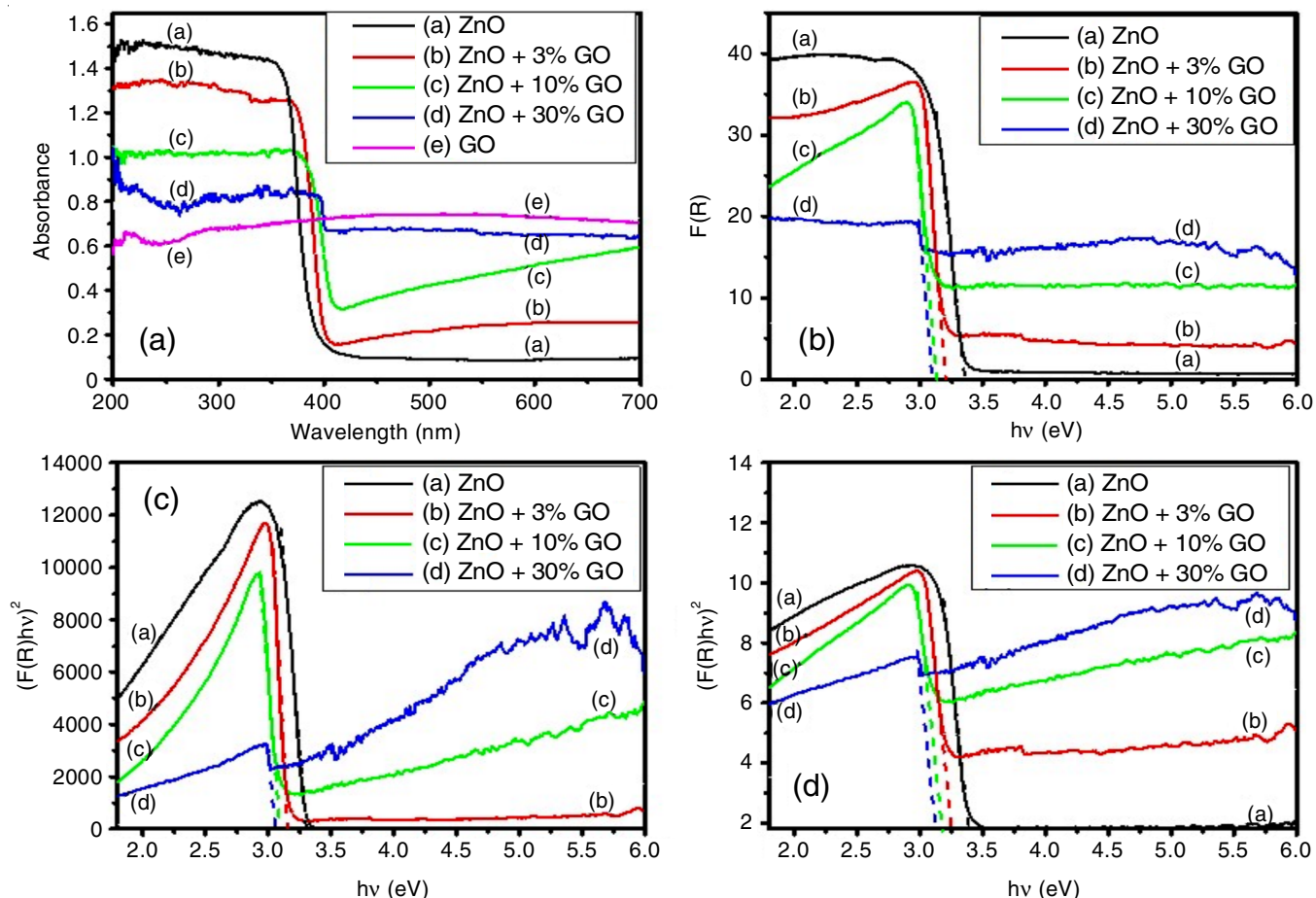

Fig. 5. UV-DRS of ZnO, GO and ZnO-GO composites (a). Optical bang gap energies of ZnO-GO composites in comparison with that of ZnO (b, c and d)

$$F(R) = \frac{(1-R)^2}{2R} \qquad (1)$$

where R is the reflectance.

The determined F(R) values were plotted against energy of radiation (hν) in eV (h = Plank's constant and ν = frequency of radiation) and from the resulting graph, E_g was determined. Values of E_g could easily be determined from the graph by extrapolating the linear portion of curve towards the *x*-axis (hν) (Fig. 5b). The E_g in eV hence obtained from F(R) *versus* hν plot was irrespective of direct or indirect transitions. Similarly, from the plotes of $(F(R)\,hν)^2$ *versus* hν and $(F(R)\,hν)^{1/2}$ *versus* hν, values of E_g corresponding to direct allowed as well as indirect allowed transitions respectively were determined (Fig. 5c-d). The values of E_g of ZnO and ZnO-GO composites using different methods are shown in Table-4. From Table-4, it was found that the value of E_g in the ZnO-composites were lower than that of pristine ZnO. Among ZnO-GO composites, as the percentage of GO increased (*i.e.* from ZnO-3% GO to ZnO-30% GO), the value of E_g further decreased. The optical property of ZnO was hence modified upon GO coupling. In ZnO-30% GO the value of E_g was almost near to the frequency of visible region. This observation supports the possibility of extension of photocatalytic activity of ZnO-GO composites in the visible region of spectra in addition to UV region.

Photodegradation studies: Through the GPC analysis details about average molecular weights and chain scissions of PS, PS-ZnO and PS-ZnO-GO composites were obtained, before and at regular intervals of UV irradiation. Number

TABLE-4
OPTICAL BANDGAP ENERGIES (eV)
OF ZnO AND ZnO-GO COMPOSITES

Method	Band gap energy (eV)			
	ZnO	ZnO + 3% GO	ZnO + 10% GO	ZnO + 30% GO
F(R) *vs.* hν	3.35	3.21	3.12	3.08
$(F(R)hν)^2$ *vs.* hν	3.30	3.16	3.09	3.05
$(F(R)hν)^{1/2}$ *vs.* hν	3.38	3.25	3.17	3.11

average molecular weight $\overline{M}_n$ and weight average molecular weight $\overline{M}_w$ of PS and PS-composites decreased as the time of UV irradiation increased attributing to the chain scission of PS chain (Fig. 6a-b). Number of chain scission per molecule S and number of scission events per gram N_t were determined using eqns. 2 and 3:

$$S = \left(\frac{\left(\overline{M}_n\right)_o}{\left(\overline{M}_n\right)_t} - 1 \right) \qquad (2)$$

$$N_t = \left(\frac{1}{\left(\overline{M}_n\right)_t} - \frac{1}{\left(\overline{M}_n\right)_0} \right) \qquad (3)$$

where $(\overline{M}_n)_0$ and $(\overline{M}_n)_t$ represents number average molecular weight of PS/PS-composites before UV exposure and after t hours of UV irradiation respectively.

S and N_t of PS-ZnO-GO composites increased more rapidly than that of pristine PS as well as PS-ZnO composite upon UV
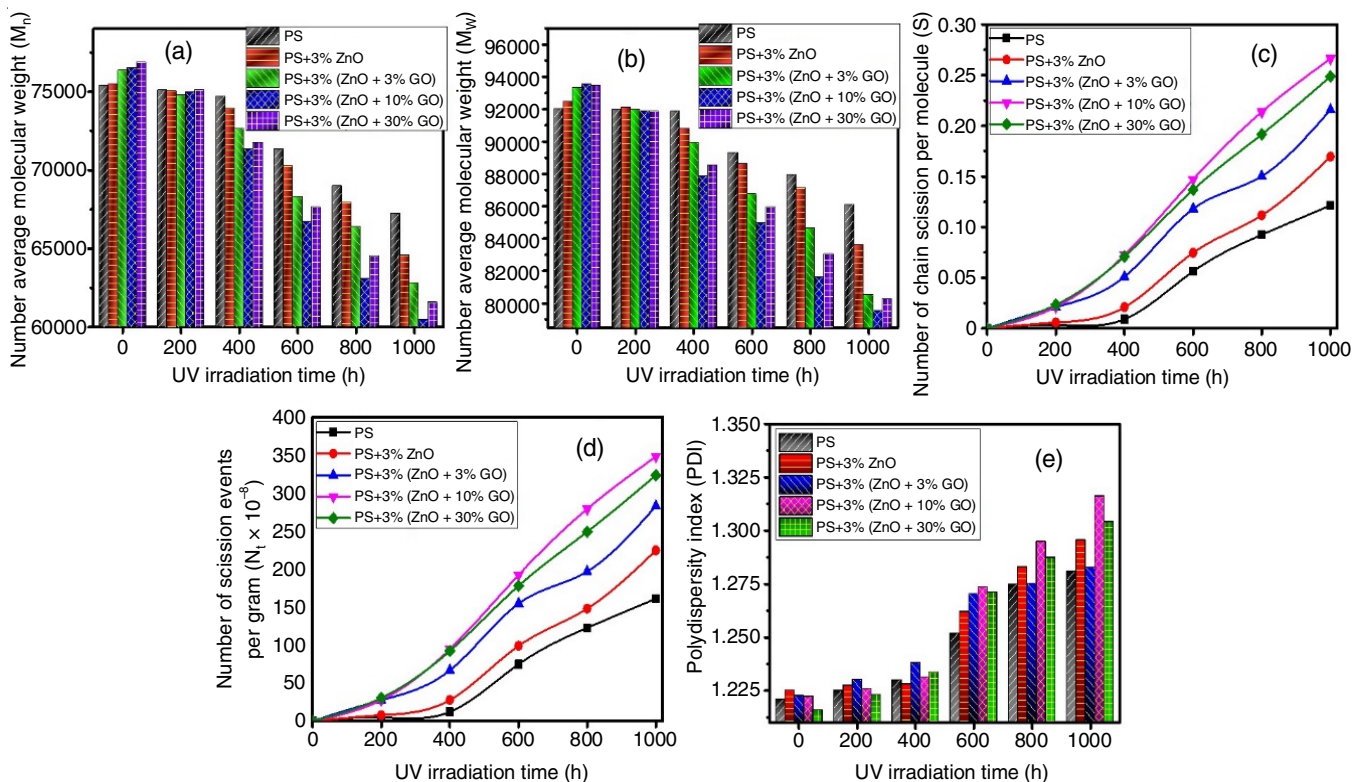

Fig. 6. Number average molecular weight $\overline{M}_n$ (a), weight average molecular weight $\overline{M}_w$ (b), number of chain scission per molecule S (c), number of scission events per gram N_t (d) and polydispersity index PDI (e) of PS-ZnO and PS-ZnO-GO composites before and after regular intervals of UV irradiation

irradiation (Fig. 6c-d). Among PS-ZnO-GO composites, predominant increase in S and N_t were observed in PS-3% (ZnO-10% GO). Polydispersity index (PDI) of the composites were determined using the following relation (eqn. 4).

$$PDI = \frac{\overline{M_w}}{\overline{M_n}} \qquad (4)$$

The observed increase in the values of PDI in PS and PS-composites upon UV exposure could be due to the increase in randomness of PS chain scission.

The alterations in the chemical structure experienced by PS/PS-composites due to UV exposure can be elucidated by FTIR spectroscopy (Figs. 7-9). FTIR spectra of PS/PS-composites taken at regular intervals of UV irradiation showed an increase in intensity of bands corresponding to carbonyl C=O (1740-1700 cm^{-1}), hydroxyl O-H/hydroperoxy OO-H (3700-3450 cm^{-1}), alkenic C=C (1680-1650 cm^{-1}) and conjugated C=C (1630-1600 cm^{-1}), stretching vibrations. The observed increase in intensities of these vibrational bands, suggests photodegradation of PS chain by photo-oxidation. As the time of UV irradiation increased, the observed increase in oxygen containing groups (>C=O, -OH and -OOH) attributes to photo-oxidation by oxygen addition whereas the increase in alkenic double bonds (C=C) and conjugated double bonds suggests photo-oxidation by hydrogen elimination. Another striking observation made from the FTIR spectra was that the bands corresponding to C-H out of plane bending of phenyl ring (centred at 1025, 907, 750 and 690 cm^{-1}) and aromatic C=C (Ar-C=C) stretch (1500 cm^{-1}) remained unaltered upon UV exposure. This observation reveals the fact that the aromatic phenyl ring of PS remain intact upon UV exposure and all the photo-oxidation occurred in the chain of PS. It could be seen that PS-ZnO-GO composites underwent better photo-oxidative degradation compared to that of pristine PS and PS-3% ZnO. Among the PS-ZnO-GO composites, the maximum photo-oxidation was observed in PS-3% (ZnO-10% GO) (Fig. 9), which was even greater compared to that of PS-3% (ZnO-30 % GO) (Fig. 10).

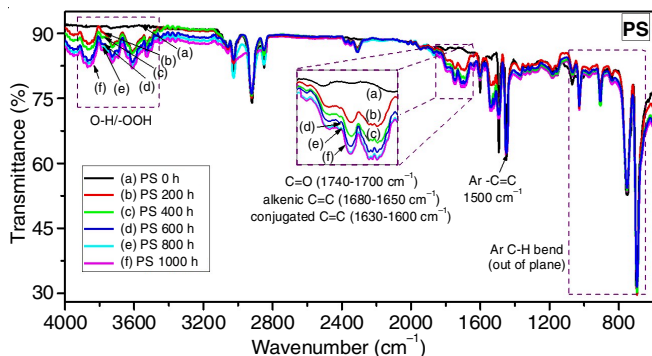Fig. 7.   FTIR spectra of PS before (a) and after regular UV exposure time intervals ranging from 200 h to1000 h (b-f)

From UV-visible diffused reflectance spectroscopy (UV-DRS) it was seen that PS-ZnO-GO composites extended the absorption of PS and PS-ZnO to the visible region of spectra (Fig. 11). With the increase in UV exposure time, four notable
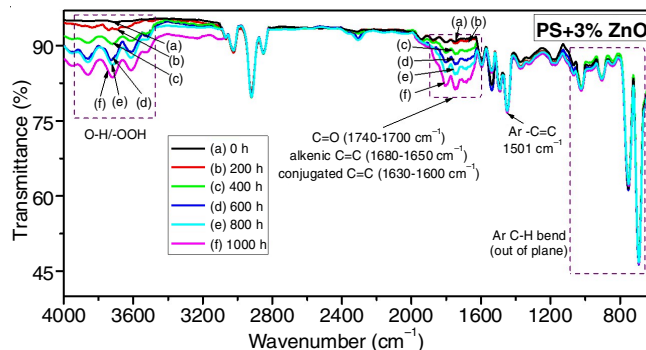

Fig. 8.   FTIR spectra of PS-3% ZnO before (a) and after regular UV exposure time intervals ranging from 200 h to1000 h (b-f)
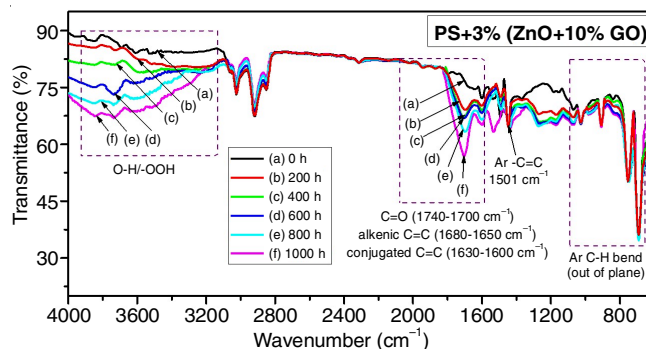

Fig. 9.   FTIR spectra of PS-3% (ZnO-10% GO) before (a) and after regular UV exposure time intervals ranging from 200 h to1000 h (b-f)
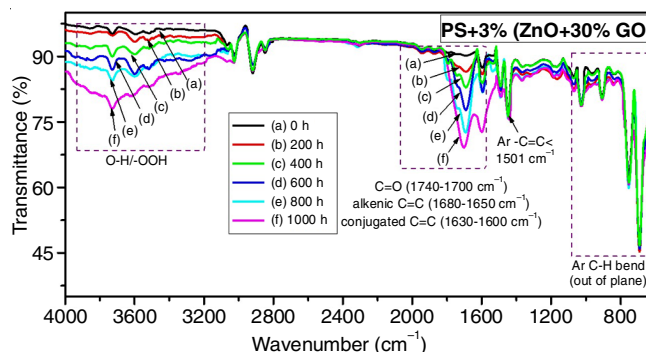

Fig. 10.   FTIR spectra of PS-3% (ZnO-30% GO) before (a) and after regular UV exposure time intervals ranging from 200 to 1000 h (b-f)

changes were observed in the absorption bands of PS, PS-ZnO and PS-ZnO-GO composites as stated (i) The intensity of characteristic absorption bands observed in the UV region (230-400 cm^{-1}) decreased, (ii) a slight increase in intensity of absorption bands were observed in the visible region (400-800 cm^{-1}), (iii) Red shift occurred in the UV region of spectra and (iv) alight increase in the absorption bands occurred in the UV region below 230 nm wavelength. It should be noted that associative interaction between the phenyl rings lead to the characteristic absorption of PS in the UV region. During UV irradiation, PS undergoes chain scission. Due to this, the effective interaction between phenyl rings within PS chain may be effected leading to a decrease in absorption intensity in the UV region. Increase in intensity of absorption in the visible region and bathochromic shift in the UV region supports the formation of conjugated carbon-carbon double bonds that
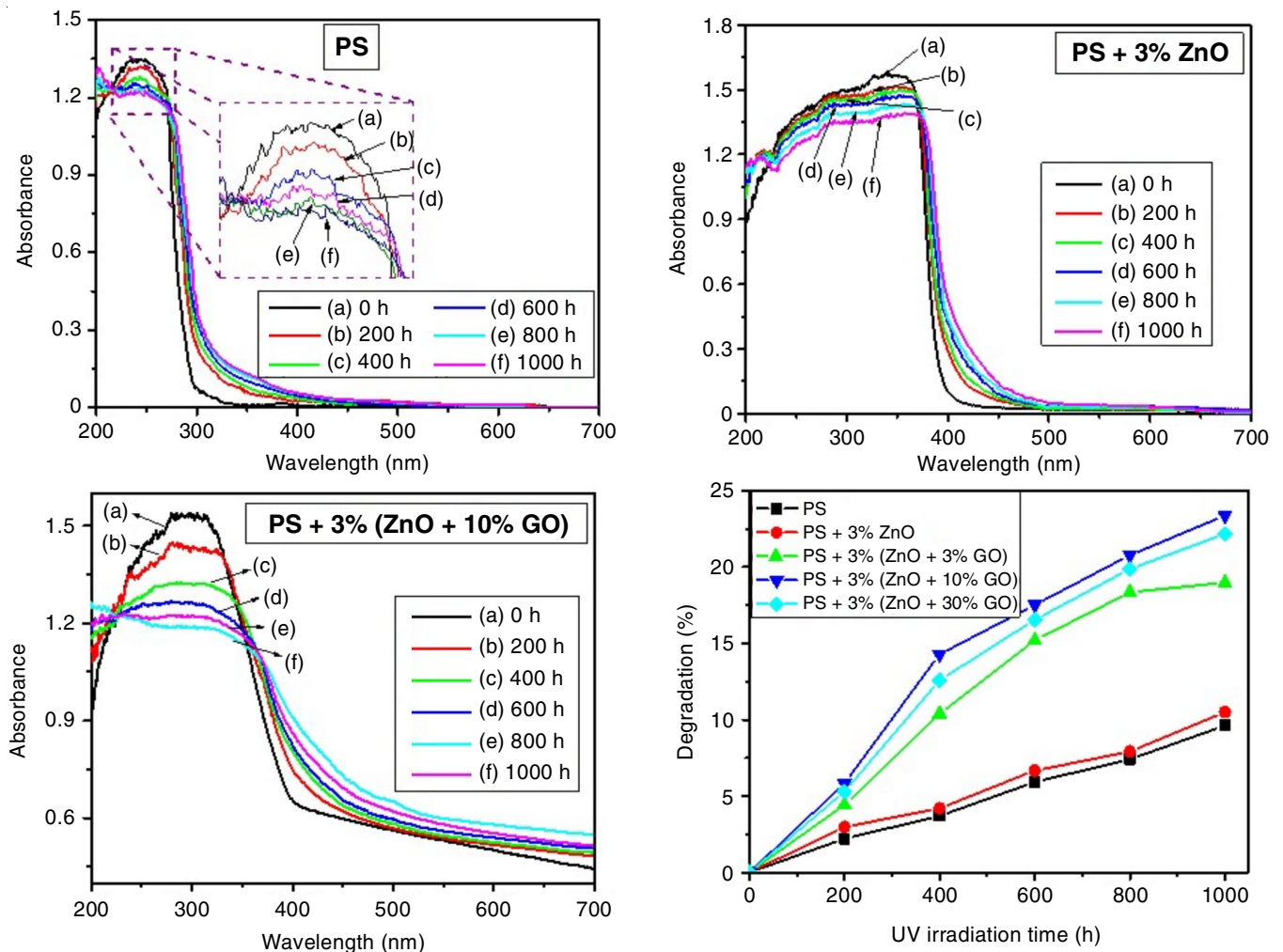
Fig. 11.   UV-DRS showing absorption and D% of PS, PS-3% ZnO, PS-ZnO-GO composites after regular intervals of UV exposure (0 to 1000 h)

absorbs visible light. The hyperchromic shift observed below 230 nm attributes to groups like -C=O, -C=C- and -OH formed due to photooxidation of PS. Thus, the observable trends were predominant in PS-ZnO-GO composites compared to PS and PS-ZnO. Among the the PS-ZnO-GO composites, PS-3% (ZnO-10% GO) underwent superior degradation and the degradation percentages (D%) of PS and PS composites were calculated from eqn 5:.

$$D\ (\%) = \left(\frac{A_o - A_t}{A_o}\right) \times 100 \tag{5}$$

where A_0 and A_t represents the absorption maxima of the specimens before and after time t of UV irradiation, respectively.

As from Fig. 11, it was found that D% was higher in PS-3% (ZnO-10% GO) compared to pristine PS and other PS composites under study. Direct bandgap energy (E_g) of the PS and PS-composites were determined using Tauc plot constructed from the following relation (eqn. 6) [43]:

$$\alpha h\nu = A(h\nu - E_g)^2 \tag{6}$$

where α is the absorption coefficient, $h\nu$ is the photon energy in eV, A is a constant (depending upon transitions), E_g is the bandgap energy.

E_g was determined by extrapolating the curve in the graph obtained by plotting $(\alpha h\nu)^2$ *versus* $h\nu$, toward *x*-axis (Fig. 12). The values of E_g of PS and PS-composites under study decreased upon UV irradiation (Table-5). The formation of conjugated double bonds and other species as a consequence of photodegradation might be the reason for the shift in their E_g to lower value.

Weight loss occurred in all the specimens under study upon UV irradiation. It could be seen from Fig. 13 that the weight loss was more predominant in PS-ZnO-GO composites and PS-3% (ZnO-10% GO) underwent maximum weight loss as expected. Gases like CO, CO_2 or even water vapours formed during photodegradation of PS chain results in such a weight loss. Carbon centred radicals are produced on polymer chain, due to the diffusion of active radical species like $H^\bullet$, $O_2^\bullet$, $OH^\bullet$ and $OH_2^\bullet$, in the presence of UV radiation [44]. These radical carbon centre then undergoes cleavage with oxygen incorporation leading to the formation of CO, CO_2 gases that escape from the matrix resulting in weight loss. Water vapours are also formed in the polymer matrix by the interaction of $H^\bullet$ and $O_2^\bullet$ [45].

Mechanical properties: Tensile strength and flexural strength of PS-ZnO and PS-ZnO-GO composites were greater
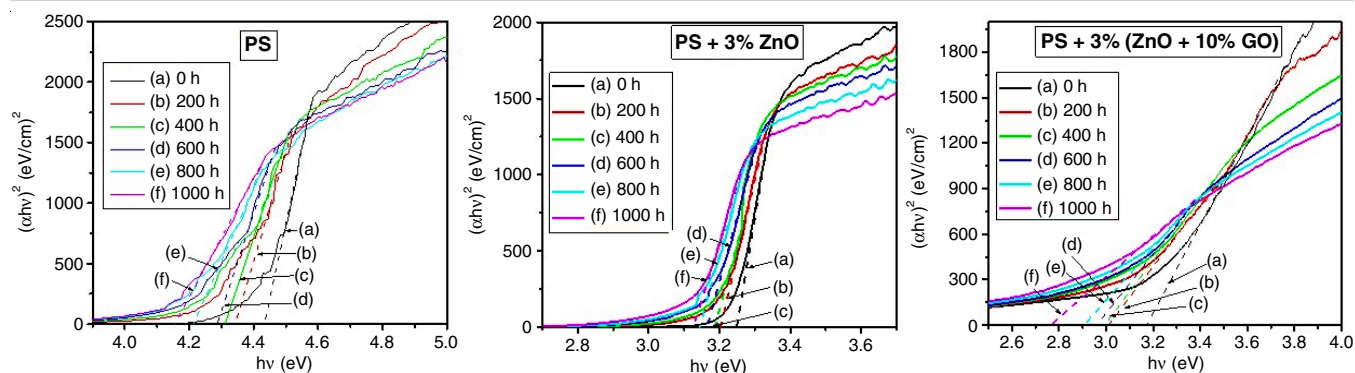
Fig. 12. E_g of PS and PS-composites determined using Tauc plote after regular intervals of UV exposure (0 to 1000 h)

TABLE-5
OPTICAL BANDGAP ENERGIES (eV) OF PS, PS-ZnO AND PS-ZnO-GO
COMPOSITES DETERMINED AT REGULAR INTERVALS OF UV IRRADIATION

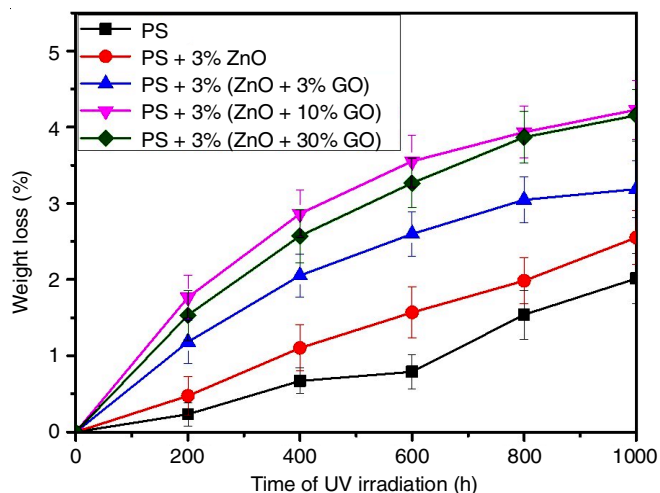| UV irradiation time (h)	Band gap energy (eV)				
	PS	PS + 3% ZnO	PS + 3% (ZnO + 3% GO)	PS + 3% (ZnO + 10% GO)	PS + 3% (ZnO + 30% GO)
0	4.43	3.25	3.22	3.18	3.16
200	4.34	3.20	3.11	3.01	2.98
400	4.31	3.19	3.07	2.99	2.92
600	4.29	3.17	2.97	2.96	2.86
800	4.21	3.14	2.90	2.90	2.79
1000	4.16	3.13	2.86	2.77	2.74

Fig. 13. Weight loss percentages of PS and PS-composites at regular intervals of UV irradiation

than that of pristine PS (Fig. 14). The enhancement in mechanical properties could explain strong binding between PS and ZnO/ZnO-GO. The superior mechanical properties exhibited by PS-composites compared to that of pristine PS, open up the scope of these composites in applications where better material strength are required. As the time of UV irradiation increased, the mechanical properties decreased in PS, PS-ZnO and PS-ZnO-GO composites. The decrease in mechanical properties may be explained by the weakening of polymer chain due to chain scission upon UV irradiation. From Fig. 14, it is also evident that PS-ZnO-GO composites underwent maximum decrease in the mechanical strength upon UV irradiation. Decrease in the mechanical strength was predominant in PS-3% (ZnO-10% GO) compared to others.

Electrical property: The dielectric breakdown of PS/PS-composites were measured at regular intervals of UV irradiation. The value of dielectric breakdown of pristine PS measured under alternating current (50 Hz) was 25.17 kV/mm (Fig. 15). An increased value (29.11 KV/mm) was obtained for PS-3% ZnO composite. This observed increase in dielectric permittivity may be due to electron trapping and scattering interfaces present between PS and ZnO that restricts easy flow of electrons [46]. However, a decrease in the value was observed in PS-ZnO-GO composites as the percentage of GO increased. GO being conductive, minimizes the dielectric breakdown voltage of the composites. As the time of UV irradiation increased, the dielectric permittivity of all the specimens under study decreased. This could be due to the formation and accumulation of various ionic and radical species within the polymer matrix, as a consequence of photodegradation of PS chain. These ionic/radical species in fact act as charge centres that facilitates easy flow of electron under applied potential. The decrease in dielectric permittivity was predominant in the PS-ZnO-GO composites compared to PS/PS-ZnO.

Thermal property: The PS, PS-3% ZnO and PS-3% (ZnO-10% GO) materials were subjected to TGA in nitrogen atmosphere. The specimens exhibited a first stage weight loss at around 116 ℃ attributing to desorption of water molecules. The second stage weight loss corresponds to the decomposition of polymer matrix. For pristine PS, the decomposition temperature was 250-395 ℃. An increase in this value was observed in PS + 3% ZnO (270-380 ℃) and PS-(ZnO-10% GO) (315-430 ℃). The increase in decomposition temperature confirms the increased thermal stability of PS upon ZnO and ZnO-GO loading. A decreased in the decomposition temperature was observed for the specimens after 1000 h of UV exposure. This
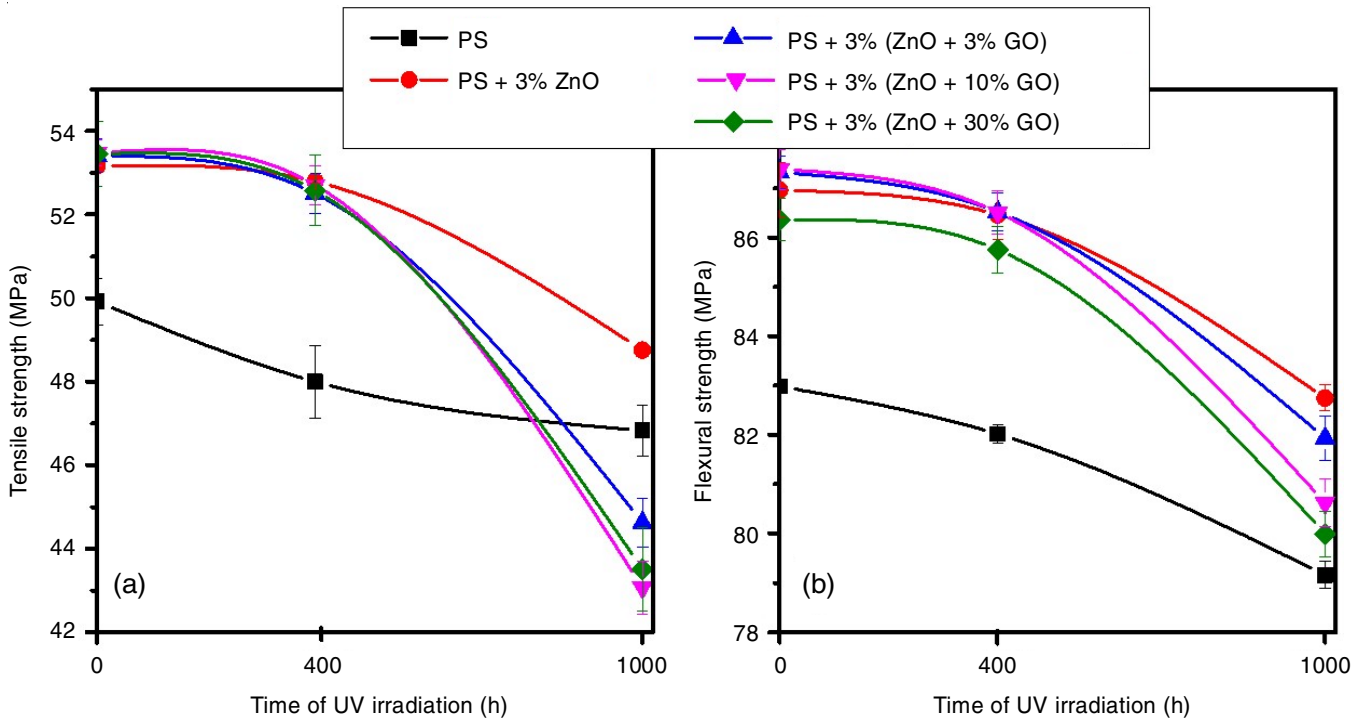
Fig. 14. Tensile (a) and flexural (b) properties of PS and PS-Composites at regular intervals of UV irradiation
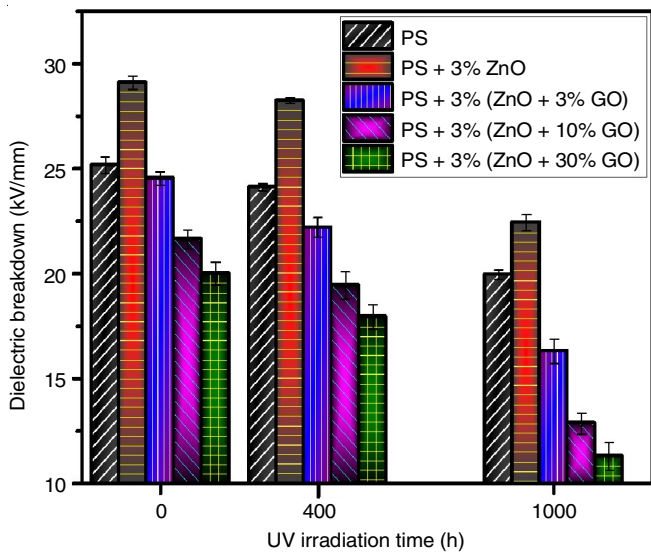

Fig. 15. Dielectric breakdown of PS and PS-composites at regular intervals of UV irradiation

could be explained on the basis of weakening or cleavage of polymer chains upon UV exposure. Thermal decomposition was predominant in PS-(ZnO-10% GO) compared to others (Fig. 16).

Mechanism of photodegradation: Polystyrene (PS) undergoes photo-oxidative degradation when exposed to UV light. In presence of UV light, phenyl rings of PS get excited into singlet excited state which may be converted into triplet excited state through inter system crossing [47]. Homolytic fission of PS chain bonds occur when excited triplet state energy of phenyl rings are transferred to PS chain. Macromolecular radicals are formed as a result of Ph-C, C-C and C-H homolytic bond cleavage. GPC analysis of PS/PS composites prove the occurrence of chain scission under UV exposure. FTIR confirms photo-oxidation of PS chain as evident from the increase in intensities of C=O, O-H/OO-H, C=C and conjugated carbon double bond vibration frequencies upon UV irradiation. It was also observed that phenyl rings of PS remain intact while the polymer chain underwent photo-oxidation and bond scission. Decrease in the
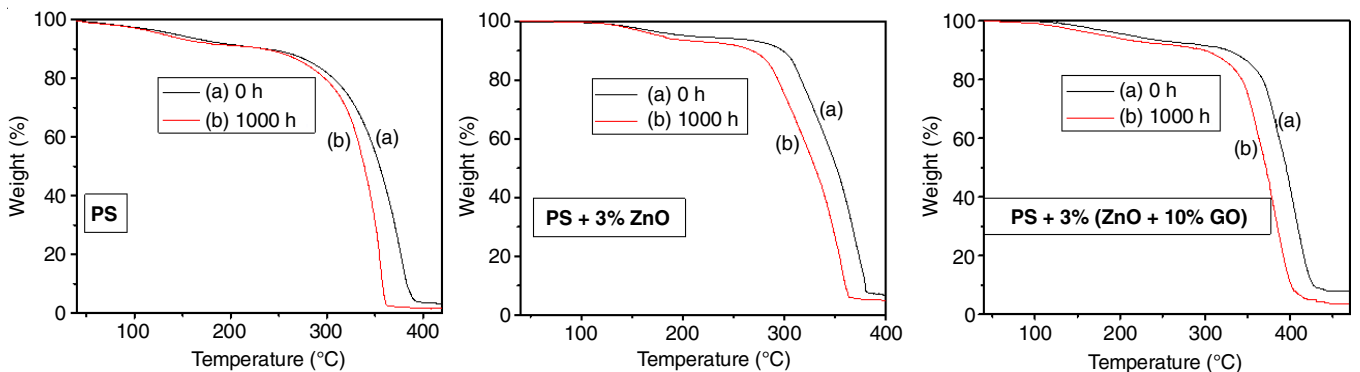

Fig. 16. TGA thermogram of PS, PS-3% ZnO and PS-3% (ZnO-10% GO) before (a) and after 1000 h (b) of UV irradiation

mechanical strength, dielectric breakdown voltage and thermal stability of UV exposed specimens highlights the fact that photodegradation has occurred in the inner polymer matrix too in addition to the exposed surface. The oxygen atoms attached covalently to the carbon atoms of PS chains during photo-oxidation is as a result of interaction of PS macromolecular with adsorbed atmospheric oxygen, in the presence of UV radiation. Formation of isolated as well as conjugated C=C double bonds are formed by elimination of hydrogen radicals (H$^\bullet$) from -CH$_2$ group of PS chain [34,40,47]. The slight yellow colour formed in the composites resulting in red shift of the absorption bands in UV irradiated specimens further supports the formation of conjugated π-bonds.

It was also evident that extend of degradation of PS increased in the presence of ZnO and ZnO-GO photocatalysts. ZnO being a semiconductor, generates electron-hole pair when exposed to UV radiation. The electrons get excited to conduction band, leaving holes in the valence band. Superoxide radical anions (O$_2^{\bullet-}$) are formed when these excited electrons interacts with adsorbed oxygen. Hydroxyl radicals (OH$^\bullet$) are formed when holes react with adsorbed water molecules [48]. O$_2^{\bullet-}$ and OH$^\bullet$ are diffused into PS matrix, accelerating photodegradation. The degradation of PS is further accelerated when ZnO-GO composites were used as photocatalysts. This observation proves the fact that the photocatalytic activity of ZnO has been further enhanced in the presence of GO. As evident from FTIR spectroscopy, a strong chemical interaction existed between ZnO and GO in ZnO-GO composites. The red shift in peak positions of C=O and C-O groups of GO supports the fact that the GO binds to ZnO through oxygen atom (of C=O and C-O). Zn-O-C bridge bond between ZnO and GO may be possibly formed. The chemical bonds between ZnO and GO facilitates easy transport of electrons from the conduction band of ZnO in excited state. These electrons are stabilized in GO through resonance [48,49]. The electrons are hence separated from holes and hence charge recombination is minimized. This increase the charge carrier life time, enhancing the photocatalytic activity of the system.

Conclusion

The modified graphene oxide-zinc oxide (ZnO-GO) composites were successfully prepared by the sonication assisted hydrothermal method. ZnO existed in hexagonal wrutzite structure as evident from powder XRD. Coupling GO with ZnO has not affected its crystal structure, however a strong chemical bonding interaction existed between ZnO and GO as evident from FTIR. The C-O and C=O vibrational bands showed a red shift in FTIR spectra in ZnO-GO composites compared to GO revealing the possibility of Zn-O-C bonds in the composites. ZnO existed as spherical like particles of dimeter about 80 nm as evident from SEM image where as in ZnO-GO composites, ZnO had hexagonal rod like structure. The HRTEM image further revealed that GO sheets held ZnO rods together and also wound around them, capping them. Optical band gap energy of ZnO decreased as the percentage of GO increased in the composites. Photodegradation of PS, PS-ZnO as well as PS-ZnO-GO composites were studies in a specially designed UV chamber that provided identical environment and uniform irradiation time. Through GPC analysis, decrease in average molecular weights and increase in chain scission were observed in PS/PS composites as UV exposure time increased. Increase in intensity of stretching vibrations corresponding to C=O, O-H, OO-H, C=C and conjugated carbon double bonds, observed in FTIR spectra supports the photo-oxidation in the composites upon UV irradiation. The UV-DRS also demonstrates the photodegradation through a considerable decrease in the characteristic absorption bands and red shift in peak positions upon irradiation. The degradation percentage of PS-ZnO-GO composites were higher compared to PS-ZnO and pristine PS. Tensile and flexural strengths of UV exposed PS/PS-composites decrease as the time of UV irradiation increased proving the fact that degradation has occurred throughout the polymer matrix. Decrease in the dielectric breakdown voltage of the specimens upon UV irradiation could be due to the formation and accumulation of various charged species. Thermal stability of the specimens too decreased upon UV irradiation. From the study, it was evident that the rate of photodegradation was higher in PS-ZnO-GO composites followed by PS-ZnO compared to pristine PS. The prepared ZnO-GO composites was hence proved to efficient photocatalyst in the degradation of PS under UV radiation. The rate of photodegradation in the PS composites, followed the order PS-(ZnO + 10% GO) > PS-(ZnO + 30% GO) > PS-(ZnO + 3% GO) > PS-ZnO > PS.

CONFLICT OF INTEREST

The authors declare that there is no conflict of interests regarding the publication of this article.

REFERENCES

1. R. Geyer, J.R. Jambeck and K.L. Law, *Sci. Adv.*, **3**, e1700782 (2017);
   https://doi.org/10.1126/sciadv.1700782
2. A.L. Brooks, S. Wang and J.R. Jambeck, *Sci. Adv.*, **4**, eaat0131 (2018);
   https://doi.org/10.1126/sciadv.aat0131
3. T.R. Walker and L. Fequet, *Trends Analyt. Chem.*, **160**, 116984 (2023);
   https://doi.org/10.1016/j.trac.2023.116984
4. B.G. Kwon, K. Saido, K. Koizumi, H. Sato, N. Ogawa, S.-Y. Chung, T. Kusui, Y. Kodera and K. Kogure, *Environ. Pollut.*, **188**, 45 (2014);
   https://doi.org/10.1016/j.envpol.2014.01.019
5. G.Q. Ali, G.A. El-Hiti, I.H.R. Tomi, R. Haddad, A.J. Al-Qaisi and E. Yousif, *Molecules*, **21**, 1699 (2016);
   https://doi.org/10.3390/molecules21121699
6. N. Chaukura, W. Gwenzi, T. Bunhu, D.T. Ruziwa and I. Pumure, *Resour. Conserv. Recycling*, **107**, 157 (2016);
   https://doi.org/10.1016/j.resconrec.2015.10.031
7. Y. Lei, H. Lei and J. Huo, *Polym. Degrad. Stab.*, **118**, 1 (2015);
   https://doi.org/10.1016/j.polymdegradstab.2015.04.005

8. F.H. Abdullah, N.H.H.A. Bakar and M.A. Bakar, *J. Hazard. Mater.*, **424**, 127416 (2022);
https://doi.org/10.1016/j.jhazmat.2021.127416

9. M. Rafique, R. Tahir, S.S.A. Gillani, M.B. Tahir, M. Shakil, T. Iqbal and M.O. Abdellahi, *Int. J. Environ. Anal. Chem.*, **102**, 23 (2022);
https://doi.org/10.1080/03067319.2020.1715379

10. M.A. Fagier, *J. Nanotechnol.*, **2021**, 6629180 (2021);
https://doi.org/10.1155/2021/6629180

11. V. Gilja, I. Vrban, V. Mandic, M. •ic and Z. Hrnjak-Murgic, *Polymers*, **10**, 940 (2018);
https://doi.org/10.3390/polym10090940.

12. S.G. Kumar and K.S.R.K. Rao, *Appl. Surf. Sci.,* **391(Part B)**, 124 (2017);
https://doi.org/10.1016/j.apsusc.2016.07.081

13. N.T. Padmanabhan, N. Thomas, J. Louis, D.T. Mathew, P. Ganguly, H. John and S.C. Pillai, *Chemosphere*, **271**, 129506 (2021);
https://doi.org/10.1016/j.chemosphere.2020.129506

14. S. Sardar, T. Munawar, F. Mukhtar, M.S. Nadeem, S.A. Khan, M. Koc, S. Manzoor, M.N. Ashiq and F. Iqbal, *Mater. Sci. Eng. B*, **288**, 116151 (2023);
https://doi.org/10.1016/j.mseb.2022.116151

15. H.-Y. Phin, Y.-T. Ong and J.-C. Sin, *J. Environ. Chem. Eng.*, **8**, 103222 (2020);
https://doi.org/10.1016/j.jece.2019.103222

16. T.V.M. Sreekanth, M.-J. Jung and I.-Y. Eom, *Appl. Surf. Sci.*, **361**, 102 (2016);
https://doi.org/10.1016/j.apsusc.2015.11.146

17. S. Lowe and Y. L. Zhong, in eds.: A.M. Dimiev and S. Eigler, Challenges of Industrial-Scale Graphene Oxide Production, In: Graphene Oxide: Fundamentals and Applications, Wiley, Chap. 13, p. 410 (2016);
https://doi.org/10.1002/9781119069447.ch13

18. D.G. Papageorgiou, I.A. Kinloch and R.J. Young, *Prog. Mater. Sci.*, **90**, 75 (2017);
https://doi.org/10.1016/j.pmatsci.2017.07.004

19. S. Kumar, S. Pratap, V. Kumar, R.K. Mishra, J.S. Gwag and B. Chakraborty, *Luminescence*, **38**, 909 (2023);
https://doi.org/10.1002/bio.4334

20. A. Kumar, K. Sharma and A.R. Dixit, *Mol. Simul.*, **46**, 136 (2020);
https://doi.org/10.1080/08927022.2019.1680844

21. H. Huang, H. Shi, P. Das, J. Qin, Y. Li, X. Wang, F. Su, P. Wen, S. Li, P. Lu, F. Liu, Y. Li, Y. Zhang, Y. Wang, Z.-S. Wu and H.-M. Cheng, *Adv. Funct. Mater.*, **30**, 1909035 (2020);
https://doi.org/10.1002/adfm.201909035

22. A. Raslan, L. Saenz del Burgo, J. Ciriza and J.L. Pedraz, *Int. J. Pharm.*, **580**, 119226 (2020);
https://doi.org/10.1016/j.ijpharm.2020.119226

23. S. Afroj, S. Tan, A.M. Abdelkader, K.S. Novoselov and N. Karim, *Adv. Funct. Mater.*, **30**, 2000293 (2020);
https://doi.org/10.1002/adfm.202000293

24. A.G. Olabi, M.A. Abdelkareem, T. Wilberforce and E.T. Sayed, *Renew. Sustain. Energy Rev.*, **135**, 110026 (2021);
https://doi.org/10.1016/j.rser.2020.110026

25. M. Shaker, R. Riahifar and Y. Li, *FlatChem*, **22**, 100171 (2020);
https://doi.org/10.1016/j.flatc.2020.100171

26. S. Wu, X. Wang, Z. Li, S. Zhang and F. Xing, *Micromachines*, **11**, 1059 (2020);
https://doi.org/10.3390/mi11121059

27. A.M. Dimiev and J.M. Tour, *ACS Nano*, **8**, 3060 (2014);
https://doi.org/10.1021/nn500606a

28. F. Farjadian, S. Abbaspour, M.A.A. Sadatlu, S. Mirkiani, A. Ghasemi, M. Hoseini-Ghahfarokhi, N. Mozaffari, M. Karimi and M.R. Hamblin, *ChemistrySelect*, **5**, 10200 (2020);
https://doi.org/10.1002/slct.202002501

29. U. Naknikham, V. Boffa, G. Magnacca, A. Qiao, L.R. Jensen and Y. Yue, *RSC Adv.*, **7**, 41217 (2017);
https://doi.org/10.1039/C7RA07472G

30. P.N.O. Gillespie and N. Martsinovich, *ACS Appl. Mater. Interfaces*, **11**, 31909 (2019);
https://doi.org/10.1021/acsami.9b09235

31. D. He, Y. Li, J. Wang, Y. Yang and Q. An, *Appl. Microsc.*, **46**, 37 (2016);
https://doi.org/10.9729/AM.2016.46.1.37

32. A. Kumar, A. Bansal, B. Behera, S.L. Jain and S.S. Ray, *Mater. Chem. Phys.*, **172**, 189 (2016);
https://doi.org/10.1016/j.matchemphys.2016.01.064

33. R. Djellabi, B. Yang, Y. Wang, X. Cui and X. Zhao, *Chem. Eng. J.*, **366**, 172 (2019);
https://doi.org/10.1016/j.cej.2019.02.035

34. S. Dinoop lal, T. Sunil Jose, C. Rajesh and K.J. Arun, *Polym. Degrad. Stab.*, **184**, 109476 (2021);
https://doi.org/10.1016/j.polymdegradstab.2020.109476

35. K. Chaudhary, M. Aadil, S. Zulfiqar, S. Ullah, S. Haider, P.O. Agboola, M.F. Warsi and I. Shakir, *Fuller. Nanotub. Carbon Nanostruct.*, **29**, 915 (2021);
https://doi.org/10.1080/1536383X.2021.1917553

36. P. Rai and Y. Yu, *Sens. Actuators B Chem.*, **173**, 58 (2012);
https://doi.org/10.1016/j.snb.2012.05.068

37. D. Chen, L. Zou, S. Li and F. Zheng, *Sci. Rep.*, **6**, 20335 (2016);
https://doi.org/10.1038/srep20335

38. M. Khannam, S. Sharma, S. Dolui and S.K. Dolui, *RSC Ad.*, **6**, 55406 (2016);
https://doi.org/10.1039/C6RA07577K

39. K.S. Lee, C.W. Park, S.J. Lee and J.-D. Kim, *J. Alloys Compd.*, **739**, 522 (2018);
https://doi.org/10.1016/j.jallcom.2017.12.248

40. S.D. Lal, T.S. Jose, C. Rajesh, P.A.R. Puthukkara, K.S. Unnikrishnan and K.J. Arun, *Eur. Polym. J.*, **153**, 110493 (2021);
https://doi.org/10.1016/j.eurpolymj.2021.110493

41. H. Arami, M. Mazloumi, R. Khalifehzadeh and S.K. Sadrnezhaad, *Mater. Lett.*, **61**, 4559 (2007);
https://doi.org/10.1016/j.matlet.2007.02.051

42. R. López and R. Gómez, *J. Sol-Gel Sci. Technol.*, **61**, 1 (2012);
https://doi.org/10.1007/s10971-011-2582-9

43. A.M. Abdelghany, E.M. Abdelrazek, S.I. Badr and M.A. Morsi, *Mater. Des.*, **97**, 532 (2016);
https://doi.org/10.1016/j.matdes.2016.02.082

44. D. Hwang, Y. Shul and Y. Chu, *Polym. Compos.*, **36**, 1462 (2015);
https://doi.org/10.1002/pc.23052

45. S. Cho and W. Choi, *J. Photochem. Photobiol. Chem.*, **143**, 221 (2001);
https://doi.org/10.1016/S1010-6030(01)00499-3

46. D. Wang, M. Huang, J. Zha, J. Zhao, Z. Dang and Z. Cheng, *IEEE Trans. Dielectr. Electr. Insul.*, **21**, 1438 (2014);
https://doi.org/10.1109/TDEI.2013.004329

47. S.D. Lal, T.S. Jose and C. Rajesh, *Environ. Nanotechnol. Monit. Manag.*, **12**, 100229 (2019);
https://doi.org/10.1016/j.enmm.2019.100229

48. A.A. Yaqoob, N.H. Mohd Noor, A. Serrà and M.N.M. Ibrahim, *Nanomaterials*, **10**, 932 (2020);
https://doi.org/10.3390/nano10050932

49. B. Tang, H. Chen, H. Peng, Z. Wang and W. Huang, *Nanomaterials*, **8**, 105 (2018);
https://doi.org/10.3390/nano8020105